

# Cisplatin-Tethered Gold Nanoparticles That Exhibit Enhanced Reproducibility, Drug Loading, and Stability: a Step Closer to Pharmaceutical Approval?

Gemma E. Craig,<sup>†</sup> Sarah D. Brown,<sup>†</sup> Dimitrios A. Lamprou,<sup>†</sup> Duncan Graham,<sup>‡</sup> and Nial J. Wheate<sup>\*,†,§</sup>

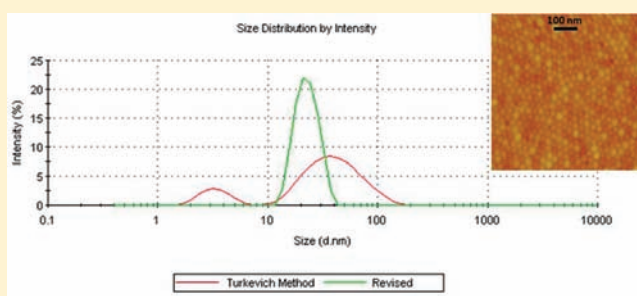
<sup>†</sup>Strathclyde Institute of Pharmacy and Biomedical Sciences, Arbutnott Building, University of Strathclyde, 161 Cathedral Street, Glasgow G4 0RE, United Kingdom

<sup>‡</sup>Centre for Molecular Nanometrology, Department of Pure and Applied Chemistry, University of Strathclyde, Thomas Graham Building, 295 Cathedral Street, Glasgow G1 1XL, United Kingdom

<sup>§</sup>Faculty of Pharmacy, The University of Sydney, Sydney, New South Wales 2171, Australia

## Supporting Information

**ABSTRACT:** Gold nanoparticles (AuNPs) can be used as delivery vehicles for platinum anticancer drugs, improving their targeting and uptake into cells. Here, we examine the appropriateness of different-sized AuNPs as components of platinum-based drug-delivery systems, investigating their controlled synthesis, reproducibility, consistency of drug loading, and stability. The active component of cisplatin was tethered to 25, 55, and 90 nm AuNPs, with the nanoparticles being almost spherical in nature and demonstrating good batch-to-batch reproducibility ( $24.37 \pm 0.62$ ,  $55.2 \pm 1.75$ , and  $89.1 \pm 2.32$  nm). The size distribution of 25 nm AuNPs has been significantly improved, compared with a previous method that produces polydispersed nanoparticles. Attachment of platinum to the AuNP surface through a poly(ethylene glycol) (PEG) linker exhibits an increase in the drug loading with increasing particle size: 25 nm ( $815 \pm 106$  drug molecules per AuNP), 55 nm ( $14216 \pm 880$ ), and 90 nm ( $54487 \pm 15996$ ). The stability of the naked, PEGylated, and platinum-conjugated nanoparticles has been examined over time under various conditions. When stored at 4 °C, there is minimal variation in the diameter for all three AuNP sizes; variation after 28 days for the 25 nm AuNPs was 2.4%; 55 nm, 3.3%; and 90 nm, 3.6%. The 25 nm AuNPs also demonstrate minimal changes in UV–visible absorbance over the same time period.



## INTRODUCTION

Cisplatin, *cis*-diamminedichloridoplatinum(II), is the leading metal drug used in the systemic treatment of solid tumors.<sup>1</sup> Its clinical use is limited by severe toxic side effects, attributed to the indiscriminate accumulation of the drug in both normal and cancerous tissue, its nonspecific interactions with extra- and intracellular proteins, and drug resistance, both intrinsic and acquired.<sup>2</sup> The focus of drug development is now being directed toward delivery vehicles that can overcome these limitations and can specifically target cancerous cells.

Because of the unique disorganized vasculature of cancer cells with numerous pores, coupled with compromised lymphatic drainage, nanoparticles can passively target solid tumors, leading to an enhanced permeability and retention (EPR) effect.<sup>3</sup> This EPR effect can be utilized by nanotechnology-based drug delivery because it enhances the accumulation of the drug in tumors and minimizes uptake by healthy cells.<sup>4</sup> For optimal efficacy, nanoparticle-based systems must take into consideration the gaps in the tumor vasculature endothelium, which can range from 100 nm to 2  $\mu$ m,<sup>5</sup> and nanoparticle clearance, which varies with the nanoparticle size.<sup>6</sup>

Gold nanoparticles (AuNPs) are particularly attractive as chemotherapy delivery vehicles because they are nontoxic, biocompatible, and easily synthesized.<sup>7–12</sup> In addition to the size, their cellular uptake is dependent upon the shape and surface charge.<sup>13–15</sup> There are two important considerations in the endocytosis of AuNPs: the binding energy between the ligand and receptor and the free energy required to drive the nanoparticles into the cell.<sup>13</sup> Uptake is limited for either extremely small or large nanoparticles, with the optimal diameter reported as between 40 and 60 nm.<sup>6,13–15</sup>

We have previously shown that tethering the active component of the platinum anticancer drug oxaliplatin to a 20 nm AuNP via a thiolated PEG linker increases cytotoxicity, compared with oxaliplatin alone, and demonstrates nuclear penetration.<sup>16</sup> AuNPs and gold nanorods have also been used as platforms for the delivery of platinum(IV) prodrugs, demonstrating enhanced cellular uptake and superior cytotoxicity compared with cisplatin.<sup>17,18</sup> Cisplatin has been loaded

Received: October 11, 2011

Published: March 5, 2012

onto AuNPs of the form Au–Au<sub>2</sub>S and Au–Fe<sub>3</sub>O<sub>4</sub> for photodynamic thermal therapy and magnetically controlled delivery, respectively.<sup>19,20</sup>

Demonstrating that drugs can be tethered to nanoparticles and that these conjugates improve drug uptake and/or activity is just the first step in the long and complex drug approval process. There are a number of other crucial factors to consider that, to our knowledge, for this type of platinum-based drug-delivery vehicle have yet to be investigated. Constructing a drug–nanoparticle conjugate with reproducible size and shape that demonstrates consistent drug loading is important for its ability to be administered for therapeutic use; i.e., it ensures that the concentration of the delivered drug remains constant. Stability, during both manufacture and storage, must also be established to guarantee that the performance is unaffected and the system remains safe.

In this paper, we report the construction of platinum-tethered AuNP conjugates using the active component of the common anticancer drug cisplatin (Figure 1). This has been

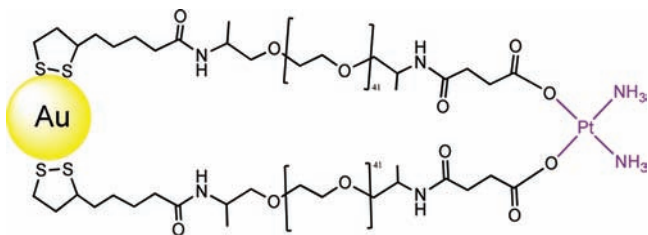


**Figure 1.** Drug–nanoparticle conjugate where the AuNP is functionalized with a PEG linker through a cyclic disulfide anchor and tethered to the active component of the anticancer drug cisplatin via the terminal carboxylate groups.

achieved for small, medium, and large AuNPs (25, 55, and 90 nm, respectively), where synthesis shows good reproducibility and monodispersity. The drug–nanoparticle conjugates have been characterized using UV–visible spectrometry, dynamic light scattering (DLS), and atomic force microscopy (AFM). The platinum drug was tethered to the AuNPs using a poly(ethylene glycol) (PEG) linker, and the drug loading was determined using inductively coupled plasma mass spectrometry (ICP-MS). Finally, we have determined the effect of the platinum drug concentration on the stability of the AuNPs during synthesis, as well as examining the growth of naked, PEGylated, and drug-conjugated nanoparticles under various conditions.

## RESULTS AND DISCUSSION

**Construction of Drug–Nanoparticle Conjugate.** The size of a AuNP can be controlled via the route of synthesis; the Brust–Schiffrin synthesis involves an organic two-phase reduction and typically yields AuNPs of 5–6 nm in diameter.<sup>21</sup> The Turkevich–Frens method of reducing a gold salt with sodium citrate has been reported to produce nanoparticles of 9–120 nm,<sup>22</sup> with larger nanoparticles in the region of 50–200 nm being produced via the reduction of HAuCl<sub>4</sub> with hydroquinone in an aqueous solution containing seeds.<sup>23</sup> Our aim was to synthesize small, medium, and large AuNPs (25, 55, and 90 nm, respectively) that demonstrate good reproducibility. This is a necessity in the construction of a drug-delivery vehicle to ensure that a consistent drug payload is being administered and that the response, whether in vitro or in vivo, can be accurately predicted.

The nanoparticles synthesized in this study have been produced from the reduction of sodium tetrachloroaurate(III) by tribasic sodium citrate, where the size of the nanoparticles is determined primarily by the pH of the solution, which, in turn, is controlled by the concentration of sodium citrate.<sup>24</sup> In this method, sodium citrate functions as both the nucleating and growth agent,<sup>7</sup> as well as distributing a negative charge on the nanoparticle surface to minimize aggregation. A higher citrate concentration allows for stabilization of smaller particles, while at lower concentrations, the coverage is incomplete, and a coarsening process leads to aggregation, producing larger particles.<sup>22</sup> These larger nanoparticles have been shown to sometimes be polydispersed and yield low particle concentrations.<sup>25</sup>

Nanoparticles, 25 nm in diameter, were initially synthesized via the established citrate reduction method.<sup>7,26</sup> This, however, produced a bimodal size distribution curve, as determined by DLS, with peaks at 3.4 and 45.4 nm (Figure 2). This is problematic because it is only with monodispersed systems that a reliable and precise dosage of drugs can be assured. A reactant concentration study, where we varied the volume of the citrate solution, led to the development of a new method for synthesizing 25 nm AuNPs demonstrating monodispersity (Figure 2) and better reproducibility (Table 1). For both the old method (Turkevich–Frens) and our revised method, the concentrations (% w/v) of the gold salt and citrate solutions remain the same; however, using a 2.7-fold increase in the volume of the citrate solution, we reproducibly synthesize spherical, monodispersed 25 nm AuNPs.

Methods to synthesize 55 and 90 nm gold were also developed, and as expected, lower concentrations of citrate were required to produce nanoparticles of these sizes. The

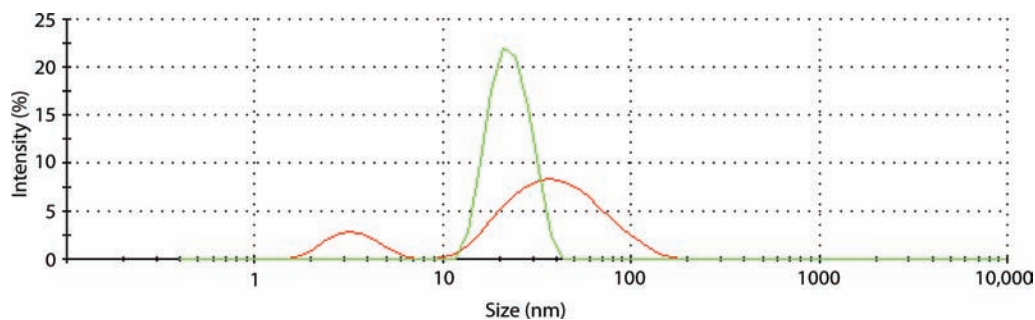


**Figure 2.** DLS spectra showing the diameter and distribution of 25 nm AuNPs synthesized via the established Turkevich–Frens method,<sup>7,26</sup> (peaks at 3.4 and 45.4 nm) and our revised method, with the latter showing monodispersity (peak average of 24.4 nm).

**Table 1. Reproducibility of 25 nm AuNPs Produced by the Two Synthetic Methods, Where the Mean Hydrodynamic Diameter (z-avg.) and the Highest Peak from the Intensity Particle-Size-Distribution Curve (i.e., the Relative Percentage of Light Scattered by Particles of Different Diameters) Were Determined by DLS: Results from Three Batches of AuNPs Demonstrating the Improved Size Reproducibility of Our Revised Method**

method	average particle diameter (nm)	highest intensity peak (nm)
Turkevich–Frens	17.9 ± 4.1	46.6 ± 4.9
revised	22.9 ± 0.6	24.4 ± 0.6

larger AuNP synthesis method displayed good reproducibility, as observed across five batches of AuNPs where small size variations ( $55.2 \pm 1.75$  and  $89.1 \pm 2.32$  nm) were observed. In addition, both the 55 and 90 nm AuNPs were found to show improved size uniformity compared with previous synthesis methods.<sup>26,27</sup> In the synthesis of larger AuNPs, it was noted that when the gold salt was not stored in a desiccator, there was significant variation in the size of the nanoparticles produced. This effect was also observed when water loss from the reaction vessel was not minimized, hence affecting the reactant concentration and altering the size of the AuNPs produced. Therefore, in the synthesis of 55 and 90 nm AuNPs, it is important to use an anhydrous gold salt and control water loss through evaporation.

Attachment of the active component of cisplatin, *cis*-{Pt(NH<sub>3</sub>)<sub>2</sub>}<sup>2+</sup>, to the AuNPs is facilitated through a PEG monolayer. PEG-based linkers are extensively used in the functionalization of AuNPs because they are stable and nontoxic, reduce nonspecific binding to proteins, and possess good water solubility.<sup>28</sup> A large number of PEG linkers can be accommodated because of the high surface area of AuNPs,<sup>29,30</sup> and in addition to improving the stability, circulation time, and cellular uptake, they provide an attachment site for drugs and/or cancer-targeting groups.<sup>28–31</sup> It has been shown that linkers with multithiol anchors, compared with their monothiol analogues, show enhanced stability when treated with small-molecule reducing/displacement agents such as dithiothreitol.<sup>31</sup> PEGylation of the AuNPs in this study was accomplished by agitating the linker with nanoparticles at appropriate concentrations, as determined by UV–visible spectrometry and size-dependent extinction coefficients, overnight. Experimental parameters for each size of AuNP are given (Table 2).

The final stage in the assembly of drug–nanoparticle conjugates was the coupling of the platinum drug to the PEGylated AuNPs. To facilitate this, cisplatin was first aquated to replace the chloride ligands with the more labile leaving group, water. The concentration of the drug used in this step

**Table 2. Experimental Parameters for the PEGylation and Purification of the Three Different-Sized AuNPs**

size of AuNP (nm)	concn of AuNP to be PEGylated (nM)	extinction coeff. <sup>32</sup> ( $\epsilon$ , M <sup>-1</sup> cm <sup>-1</sup> )	centrifuge settings	
			speed (rpm)	time (min)
25	17	$2.7 \times 10^8$	7000	20
55	0.17	$2.65 \times 10^{10}$		7
90	0.017	$1.346 \times 10^{11}$		2

was directly adapted from our previous study;<sup>16</sup> however, for many early batches, we found that the nanoparticles turned a blue-purple color upon the addition of platinum, measured as a red shift of  $\lambda_{\max}$  of the AuNPs or shoulders/additional peaks in the UV–visible spectra (Supporting Information). This is indicative of AuNP aggregation,<sup>33</sup> and in some cases, aggregates precipitated out of the solution and could not be resuspended. We believe that this is a result of the decreased surface charge on the nanoparticles because they go from negatively charged (from the carboxylate groups on the PEG linker) to neutral. To eliminate this problem and determine maximum platinum loading, concentration studies were performed for each of the three different-sized nanoparticles, using  $\zeta$  potential as the measure of stability (Figure 3). The results confirmed our hypothesis; with higher concentrations of platinum, a red shift of  $\lambda_{\max}$  was observed (data not shown), corresponding to the overall AuNP charge approaching zero. A linear relationship exists between the concentration of *cis*-{Pt(NH<sub>3</sub>)<sub>2</sub>}<sup>2+</sup> added and the  $\zeta$  potential, a common measurement used to indicate stability,<sup>34,35</sup> and is dependent upon the nanoparticle size (Figure 3). Aggregation and precipitation occurred at lower platinum concentrations for 55 and 90 nm AuNPs, and after precipitation, the  $\zeta$  potential could not be measured. Using the  $\zeta$  potential and the observation of whether the nanoparticles remained in solution over time, we have determined the maximum amount of aquated cisplatin that can be used in the conjugation of platinum to AuNPs, which will maintain nanoparticle stability: 25 nm,  $0.94 \times 10^{-12}$  molecules of platinum; 55,  $0.47 \times 10^{-12}$ ; 90,  $0.19 \times 10^{-12}$ .

**Nanoparticle Characterization.** The different-sized, naked, PEGylated, and drug-conjugated nanoparticles were analyzed using a number of techniques to measure the particle size, including UV–visible spectrometry, AFM, and DLS. UV–visible spectrometry shows a red shift with increasing particle diameter with a  $\lambda_{\max}$  of around 518 nm for the 25 nm AuNPs, which is characteristic of AuNPs around this size (Figure 4).<sup>36</sup> The 55 and 90 nm AuNPs have  $\lambda_{\max}$  values of around 528 and 563 nm, respectively.

To determine the particle size, the nanoparticles were analyzed in the solid state using AFM (Figure 5). The naked AuNPs are roughly spherical in shape, particularly the 25 nm AuNPs, with the larger AuNPs showing improved shape distribution compared with previous nanoparticles of comparable size synthesized via the Turkevich–Frens method.<sup>26</sup> Their size correlates well with the results obtained by DLS, with the average diameter varying by less than 9%: 24.0 and 25.37 nm; 56.7 and 55.6 nm; 97.3 and 89.2 nm (sizes determined by AFM and DLS, respectively). It should be noted that, for the 90 nm AuNPs, we would expect the hydrodynamic diameter to be larger than that obtained from AFM.

The effect of PEGylation and drug conjugation on the particle size was also determined by AFM and DLS (Figure 5). The AFM images indicate that there is no significant change in the size of the nanoparticles at any stage. Their hydrodynamic diameter in suspension, however, shows an increase in the particle size upon PEGylation and drug conjugation. The naked 25 nm AuNPs demonstrate increases from 24.4 nm in size to 35.1 and 37.4 nm after PEGylation and platinum conjugation, respectively (Figure 5). The hydrodynamic diameter of the 55 nm AuNPs increases from 55.6 nm to 73.2 and 75.9 nm and that of the 90 nm AuNPs from 89.2 nm to 107.2 and 106.0 nm upon PEGylation and conjugation, respectively. The increase in the size after PEGylation can be used to determine the

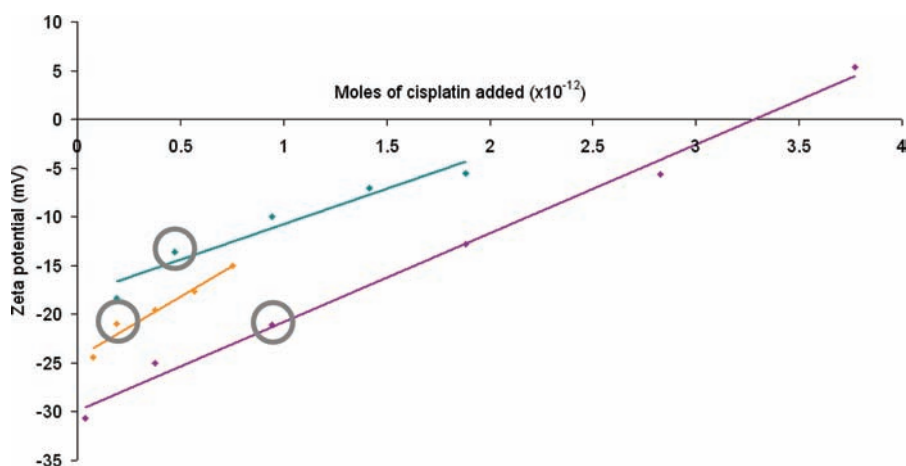


**Figure 3.** Graph showing the effect of the platinum concentration on the charge of different-sized AuNPs after drug conjugation: 25 nm (purple,  $r^2 = 0.9926$ ); 55 nm (green,  $r^2 = 0.9318$ ); 90 nm ( $r^2 = 0.9567$ ). For each size, the concentration of aquated cisplatin above which significant nanoparticle aggregation occurs is highlighted.

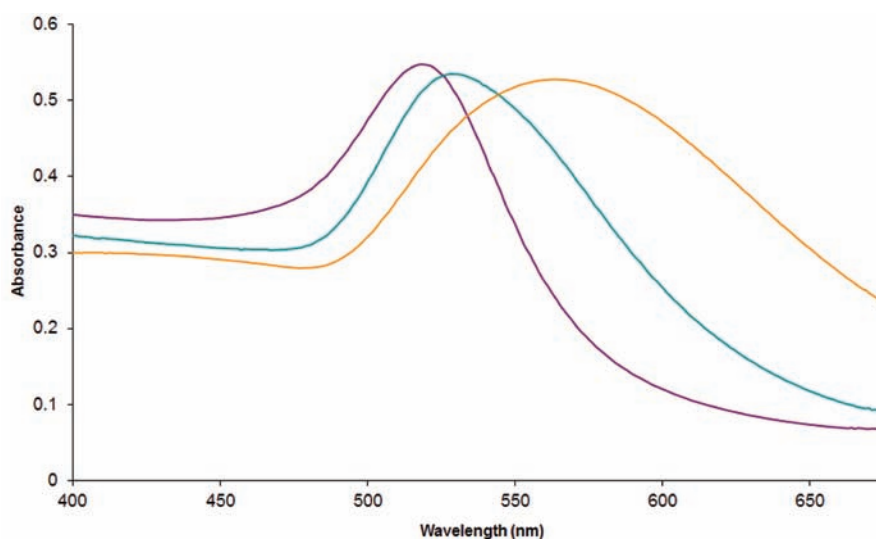


**Figure 4.** UV-visible spectra of the three different-sized AuNPs—25 nm (purple,  $\lambda_{\text{max}} = 518$  nm), 55 nm (green,  $\lambda_{\text{max}} = 528$  nm), and 90 nm (orange,  $\lambda_{\text{max}} = 563$  nm)—showing the expected red shift with increasing nanoparticle size.

thickness of the PEG layer;<sup>37</sup> however, any polydispersity in the size distribution makes this difficult.<sup>38</sup> The larger hydrodynamic diameters yielded by DLS for the latter two stages of assembly, compared to those observed for the naked AuNPs, are due to interactions between the solvent and the covalently surface-bound PEG. This effect has been previously observed for PEGylated AuNPs,<sup>39,40</sup> where hydrodynamic interactions are increased for large PEG linkers.<sup>41</sup> The polymer monolayer decreases the mobility of the nanoparticle,<sup>42</sup> most likely because of solvent interactions. The absence of aggregation when platinum is conjugated to the AuNP is an improvement on what we have previously published, where a 4.5-fold increase in the size was observed in both the solution and solid state.<sup>16</sup> This is because, previously, the platinum drug used was the active component of oxaliplatin, {Pt(1*R*,2*R*-diaminocyclohexane)}, which has a cyclohexane-based ligand and may cause aggregation through hydrophobic self-interactions. Using the active component of cisplatin introduces polar ammine ligands that can hydrogen bond with water molecules and help retain stability in solution.

**Determination of the Platinum Content.** The presence of platinum was confirmed by UV-visible spectrometry because spectra obtained were of a profile similar to those of previous studies of cisplatin in water, with a weak absorption band that can extend to 350 nm and a sharp increase in absorbance between 230 and 250 nm (Figure 6).<sup>43</sup> To quantitatively determine the number of platinum molecules per nanoparticle, the drug-nanoparticle conjugates were first digested using sodium cyanide<sup>44</sup> and subsequently analyzed by ICP-MS. We have previously been able to demonstrate drug loading of up to 300 platinum per AuNP,<sup>16</sup> with another study showing up to 2812 platinum per AuNP.<sup>20</sup>

In this study, the drug loading was found to increase significantly with increasing particle size: 25 nm ( $815 \pm 106$  drug molecules per AuNP); 55 nm ( $14216 \pm 880$ ); 90 nm ( $54487 \pm 15996$ ). The number of drug molecules conjugated to the AuNPs exhibit significant enhancement on all of those previously published. This improved high drug loading is important because it may lead to a significant increase in the dose delivered to tumors, especially in the case of the 90 nm drug-nanoparticle conjugates. If the cellular uptake and activity

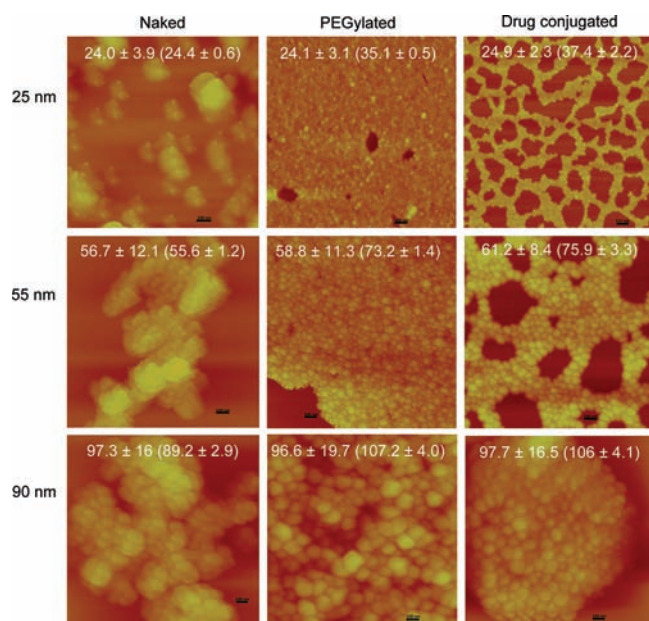


**Figure 5.** AFM images of the 25, 55, and 90 nm naked, PEGylated, and drug-conjugated AuNPs, showing the particle size as determined by AFM and their hydrodynamic diameter (in brackets) obtained by DLS. An increase in the hydrodynamic diameter is observed upon PEGylation and platinum conjugation: 25 nm, 44 and 52% (PEGylated and conjugated, respectively); 55 nm, 32 and 37%; 90 nm, 20 and 19%.

remain unaffected, the higher payload will result in increased cytotoxicity and possibly even overcome some forms of drug resistance. One issue, however, that must be resolved is the variability of the drug loading on the nanoparticles: 25 nm, 13%; 55 nm, 6%; 90 nm, 29%.

**Nanoparticle Stability.** Nanoparticle instability may manifest as agglomeration and/or particle growth, both of which result in an increase in the diameter and a red shift of  $\lambda_{\max}$  in the case of AuNPs. Maintaining stability over time is essential for the efficacy and safety of AuNP-based drugs because unstable nanosuspensions can affect administration and the dose delivered.<sup>45</sup>

A previous study that investigated the stability of 20 nm AuNPs synthesized via the Turkevich–Frens method highlighted that nanoparticle growth and precipitation from the solution are issues.<sup>46</sup> When stored at room temperature, the nanoparticles grew up to 6.5-fold in size, and at 4 °C, although growth was less than that when stored at higher temperature, the size of the nanoparticles increased to 40 nm.<sup>46</sup>

It was therefore of interest to study the stability of our AuNPs. We have used DLS to monitor changes in the hydrodynamic diameter of the nanoparticles over time, at room temperature and 4 °C. We have examined naked and PEGylated nanoparticles and, for the first time, looked at the stability of platinum-conjugated AuNPs. Compared with the previous study,<sup>46</sup> the 25 nm naked AuNPs demonstrate improved stability over a 4-week period, with average maximum diameters of 33.2 and 26.3 nm when stored at room temperature and 4 °C, respectively (Figure 7). Variation in the size for the naked nanoparticles after 28 days was 2.4%. PEGylated and drug-conjugated AuNPs also show minimal variation in the size at 4 °C, with the average diameter after 28 days demonstrating only a 2.7 and 2.3% increase in size, respectively, from the initial measurement (Figure 7). When stored at room temperature, the 25 nm nanoparticles increase by 4.0 and 15.6% in size for the PEGylated and drug-conjugated nanoparticles. The growth of the nanoparticles is therefore dependent upon storage conditions and so, to maintain stability over time, they should be stored at 4 °C. The minimized growth at this temperature is postulated to be

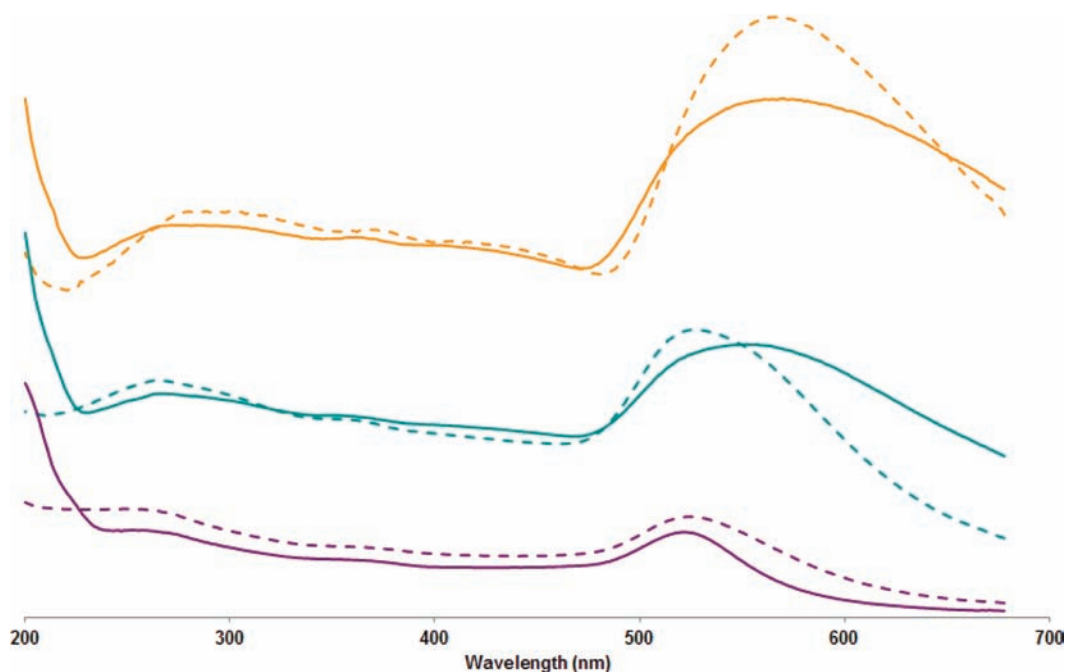


**Figure 6.** UV–visible spectra of PEGylated-only (dashed) and platinum-loaded (solid) AuNPs: 25 nm (purple), 55 nm (green), and 90 nm (orange). A red shift is observed compared with naked AuNPs (Figure 4), and upon tethering of the active component of cisplatin to the AuNPs, a sharp increase in absorbance is observed around 230 nm. Absorbance has been removed to stack spectra clearly.

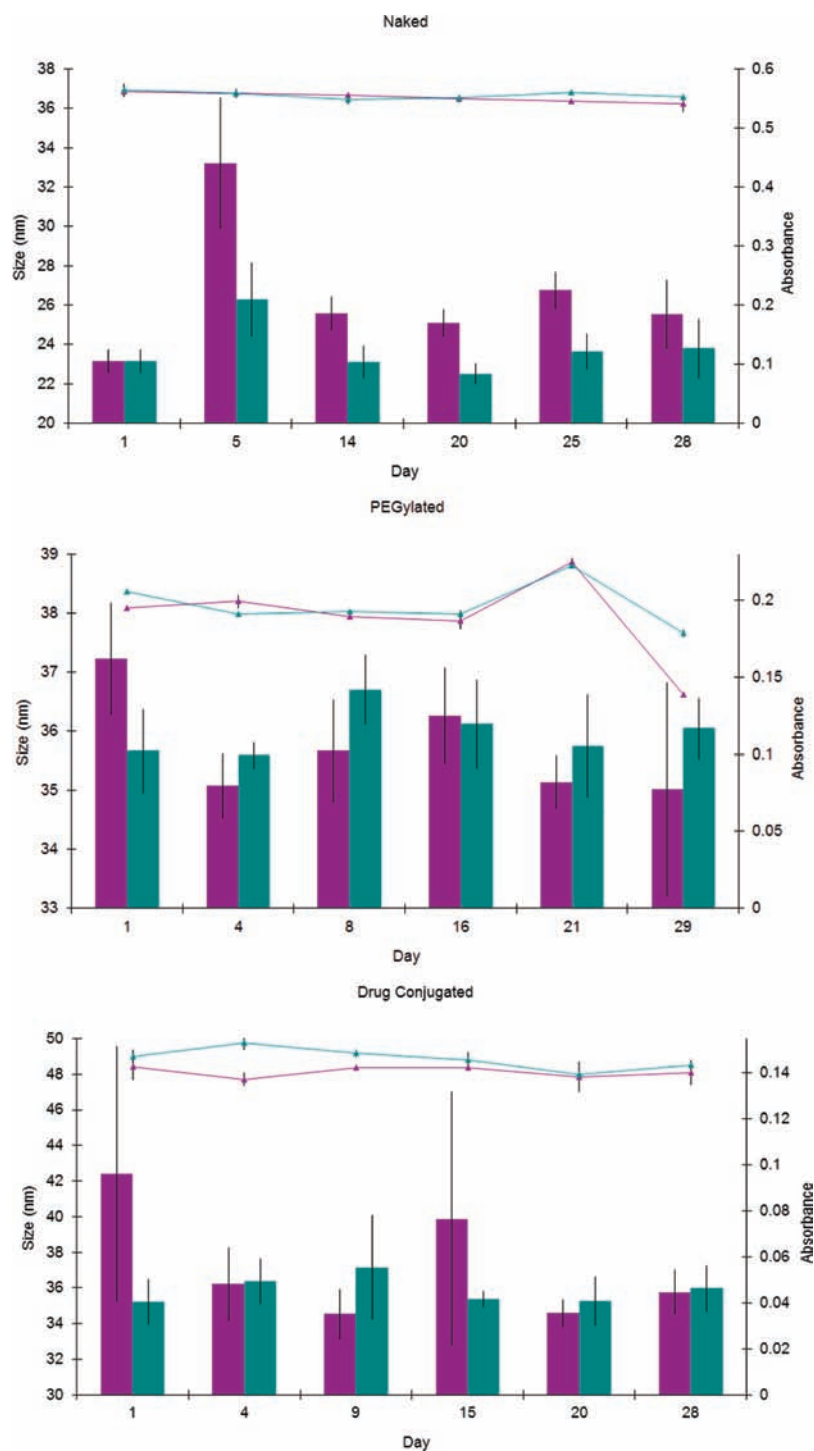


**Figure 7.** Stability of 25 nm AuNPs at each stage of assembly when stored at room temperature (purple) and at 4 °C (green), with day 1 representing the day of synthesis. The bar chart represents the nanoparticle diameter in nanometers, as measured by DLS (left axis), and the line graph is nanoparticle absorbance, as measured by UV–visible (right axis).

because, at the higher temperature, there is more kinetic energy to encourage agglomeration, which results in larger particle sizes.<sup>46</sup>

Because minimized growth was observed at 4 °C for the 25 nm AuNPs, it was this temperature at which the stability of 55 and 90 nm AuNPs was examined. For either size, minimal growth is observed, regardless of whether the nanoparticles are naked, PEGylated, or drug-conjugated (not shown). For the naked nanoparticles, variations in the average diameter after 28

days were 3.3 and 3.6% for the 55 and 90 nm AuNPs, respectively. The results from the three different-sized AuNPs show that the drug-conjugated nanoparticles exhibit enhanced stability compared with the previous two stages of assembly.

We also examined changes in UV–visible absorbance of the 25 nm AuNPs. This technique was used to assess the AuNP stability because decreases in  $\lambda_{\max}$  may have indicated that aggregation had occurred and/or the nanoparticles had precipitated. There were no drastic changes in absorbance,

except for the PEGylated nanoparticles when stored at room temperature (Figure 7). The drop in the concentration of the PEGylated AuNPs reinforces our earlier conclusion that AuNPs should be stored at low temperatures.

This investigation has established that the method we have developed for AuNP synthesis produces naked nanoparticles that are relatively stable over time. We have also demonstrated that when stored at low temperatures, 25, 55, and 90 nm naked, PEGylated, and drug-conjugated AuNPs exhibit a smaller degree of size variation over time.

## CONCLUSIONS

For any new drug to get approval for human clinical trials, it must demonstrate not only efficiency but also the capability of being reproducibly manufactured and stored in a stable manner whether the formulation is in a solid form or an aqueous suspension. Previously, we, and others, have shown that platinum drugs can be conjugated to AuNPs and that cellular uptake and cytotoxicity are significantly improved. To further develop AuNPs as platinum drug-delivery vehicles, it was essential to establish their level of reproducibility and stability. Here, we have reported a revised method for producing AuNPs that displays better size distribution and reproducibility for 25 nm AuNPs. For 55 and 90 nm AuNPs, the method shows improved nanoparticle shape and good reproducibility. Subsequent conjugation of the nanoparticles with the active component of cisplatin,  $cis\text{-}\{Pt(NH_3)_2\}^{2+}$ , showed enhanced drug loading, with the number of platinum per nanoparticle ranging from 700 to 70000. An issue that must be addressed in the future, however, is the variability of the drug loading on each of the AuNP sizes. During drug conjugation, an increase in the concentration of  $cis\text{-}\{Pt(NH_3)_2\}^{2+}$  led to an increase in the overall charge of the nanoparticle, representative of the nanosuspension becoming unstable. Additionally, it has previously been shown that AuNPs can grow and/or aggregate when stored as suspensions. We have found that storage at 4 °C and drug conjugation of the nanoparticles improves their stability so that they can be stored for several weeks without significant change. Overall, these results provide an important next step in the development of AuNPs as delivery vehicles for platinum drugs. To move forward, a large-scale synthetic method should be developed so that AuNPs and their drug conjugates can be fully examined in vitro and in vivo.

## METHODS

**Materials.** All chemicals and solvents used were purchased from Sigma-Aldrich. All aqueous solutions were prepared using water filtered by a Millipore purification unit. The synthesis of aquated cisplatin followed a published method,<sup>47</sup> as did the synthesis of the poly(ethylene glycol) (PEG) linker.<sup>16</sup>

**ICP-MS.** Before analysis, AuNPs were digested into gold ions using a standard method of dissolution with sodium cyanide.<sup>44</sup> An Agilent 7700X instrument, with a micromist nebulizer and an octapole collision cell, was calibrated using solutions prepared from a Spex CertPrep platinum standard at concentrations ranging from 0 to 1000 ppb, containing 2% nitric acid. The platinum drug concentration on the AuNPs was determined using the <sup>195</sup>Pt isotope. Instrument operating conditions used were 1550 W radio-frequency forward power, 0.85 L min<sup>-1</sup> plasma carrier gas flow, 0.2 L min<sup>-1</sup> make-up gas flow, 4.6 mL min<sup>-1</sup> helium gas flow in the collision cell, and 0.1 rps for the nebulizer pump. The sample depth was 8 mm, the sample period was 0.31 s, and the integration time was 0.1 s.

**DLS.** DLS and  $\zeta$  potential experiments were conducted on a Malvern Zetasizer Nano ZS. The machine was calibrated using a 60

nm polystyrene standard. A 1 mL sample was loaded into a cell, and the particle size and  $\zeta$  potential were measured simultaneously three times with triplicate samples.

**AFM.** A AuNP suspension (5  $\mu$ L) was deposited onto a freshly cleaved mica surface (G250-2 mica sheets 2.54 cm  $\times$  2.54 cm  $\times$  0.015 cm; Agar Scientific Ltd., Essex, U.K.) and air-dried for 30 min. The images were obtained by scanning the mica surface in air under ambient conditions using a Bruker MultiMode with NanoScope IIIA controller scanning probe microscope (Digital Instruments, Santa Barbara, CA; Bruker software version 6.14r1) operated in tapping mode. The AFM measurements were obtained using sharp silicon probes [TESP; nominal length ( $l_{nom}$ ) = 125  $\mu$ m, width ( $w_{nom}$ ) = 40  $\mu$ m, tip radius ( $R_{nom}$ ) = 8 nm, resonant frequency ( $\nu_{nom}$ ) = 320 kHz, spring constant ( $k_{nom}$ ) = 42 N m<sup>-1</sup>; Bruker Instruments SAS, Dourdan, France]. AFM scans were taken at 512  $\times$  512 pixels resolution and produced topographic images of the samples in which the brightness of the features increases as a function of the height. Typical scanning parameters were as follows: tapping frequency 322 kHz, integral and proportional gains 0.4 and 0.6, respectively, set point 0.4–0.6 V, and scanning speed 1.0 Hz. AFM images were collected from two different samples and at random spot surface sampling (at least five areas).

**UV-Visible Spectroscopy.** UV-visible spectra were obtained using a Varian Cary 50 Bio spectrophotometer running Cary WinUV scan software. Each sample (2 mL) was prepared at appropriate dilutions to achieve absorption values between 0 and 1. Samples were examined in a silica cuvette (1 cm), and an average of three measurements was used.

**Synthesis of Naked AuNPs.** All glassware used in the preparation of nanoparticles was soaked in aqua regia (3:1 HCl/HNO<sub>3</sub>) for at least 4 h and then rinsed with distilled water until the water pH was neutral. NaAuCl<sub>4</sub>·2H<sub>2</sub>O (50 mg, 0.14 mmol) was dissolved in a three-neck round-bottomed flask using distilled water (500 mL). This was heated using a bunsen burner to 100 °C with continuous stirring by a double-linked glass stirrer using a mechanical stirrer (Janke & Kunkel, type RW20, speed setting "5.5"). Each neck of the flask was sealed with tinfoil to minimize the loss of water by evaporation. Upon boiling, a fresh room temperature solution of sodium citrate was added to achieve the desired size of the nanoparticle (1% m/v stock solution: 25 nm, 20 mL; 55 nm, 3.7 mL; 90 nm, 2.1 mL). The solution was continuously boiled and stirred for 15 min before cooling to room temperature while stirring at a reduced speed (speed setting "2"). The colloid was concentrated by a centrifuge (25 nm, 6000 rpm/2 h; 55 nm, 4000 rpm/20 min; 90 nm, 4000 rpm/10 min) and the supernatant liquid removed by decanting.

**Assembly of Platinum Tethered Nanoparticles.** To an Eppendorf vessel containing AuNPs (1 mL: 25 nm, 17 nM; 55 nm, 0.17 nM; 90 nm, 0.017 nM), the PEG linker was added (100  $\mu$ L, 1 mM) and agitated for 4 h by placing it in a round-bottomed flask and spinning on a rotary evaporator. The unbound PEG linker was removed by a centrifuge (7000 rpm: 25 nm, 20 min; 55 nm, 7 min; 90 nm, 2 min), the supernatant liquid removed, and the remaining pellet resuspended in water (1 mL). The washing process was repeated once more before *N,N*-diisopropylethylamine (100  $\mu$ L, 0.1 mM) was added to the nanoparticles. This was followed by the addition of 25  $\mu$ L of a  $cis\text{-}[Pt(OH)_2(NH_3)_2]\cdot 2NO_3$  dissolved in a 1,3-dimethyl-3,4,5,6-tetrahydro-2(1H)-pyrimidone stock solution (25 nm, 10 mg mL<sup>-1</sup>; 55 nm, 5 mg mL<sup>-1</sup>; 90 nm, 2 mg mL<sup>-1</sup>), and the nanoparticle was left to agitate overnight. Finally, the AuNPs were centrifuged (same conditions as those for purification of the PEGylated nanoparticles; Table 2), the supernatant liquid was removed, and the remaining pellet was resuspended in water (1 mL) before the wash was repeated once more.

## ASSOCIATED CONTENT

### Supporting Information

Accurate particle size determination using AFM, a full UV-visible spectrum of a 25 nm naked nanoparticle, and UV-visible spectra showing the aggregation of 25 nm AuNPs. This

material is available free of charge via the Internet at <http://pubs.acs.org>.

## AUTHOR INFORMATION

### Corresponding Author

\*E-mail: [nial.wheate@sydney.edu.au](mailto:nial.wheate@sydney.edu.au). Fax: + 61 2 9351 4391.

### Notes

The authors declare no competing financial interest.

## REFERENCES

- (1) Kelland, L. *Nat. Rev. Cancer* **2007**, *7*, 573.
- (2) Wheate, N. J.; Craig, G. E.; Walker, S.; Oun, R. *Dalton Trans.* **2010**, *39*, 8097.
- (3) Matsumura, Y.; Maeda, H. *Cancer Res.* **1986**, *46*, 6387.
- (4) Couvreur, P.; Dubernet, C.; Brigger, I. *Adv. Drug Delivery Rev.* **2002**, *54*, 631.
- (5) Hobbs, S. K.; Monsky, W. L.; Yuan, F.; Roberts, W. G.; Griffith, L.; Torchilin, V. P.; Jain, R. K. *Proc. Natl. Acad. Sci. U.S.A.* **1998**, *95*, 4607.
- (6) Perrault, S. D.; Walkey, C.; Jennings, T.; Fischer, H. C.; Chan, W. C. W. *Nano Lett.* **2009**, *9*, 1909.
- (7) Turkevich, J.; Stevenson, P. C.; Hillier, J. *Discuss Faraday Soc.* **1951**, *11*, 55.
- (8) Connor, E. E.; Mwamuka, J.; Gole, A.; Murphy, C. J.; Wyatt, M. D. *Small* **2005**, *1*, 325.
- (9) Shukla, R.; Bansal, V.; Chaudhary, M.; Basu, A.; Bhonde, R. R.; Sastry, M. *Langmuir* **2005**, *21*, 10644.
- (10) Jelveh, S.; Chithrani, D. B. *Cancers* **2011**, *3*, 1081.
- (11) Lu, W.; Singh, A. K.; Khan, S. A.; Senapati, D.; Yu, H.; Ray, P. C. *J. Am. Chem. Soc.* **2010**, *132*, 18103.
- (12) Senapati, D.; Singh, A. K.; Khan, S. A.; Senapati, T.; Ray, P. C. *Chem. Phys. Lett.* **2011**, *504*, 46.
- (13) Wang, S.-H.; Lee, C.-W.; Wei, P.-K. *J. Nanobiotechnol.* **2010**, *8*, 1.
- (14) Chithrani, B. D.; Ghazani, A. A.; Chan, W. C. W. *Nano Lett.* **2006**, *6*, 662.
- (15) Jiang, W.; Kim, B. Y. S.; Rutka, J. T.; Chan Warren, C. W. *Nano* **2008**, *3*, 145.
- (16) Brown, S. D.; Nativo, P.; Smith, J.-A.; Stirling, D.; Edwards, P. R.; Venugopal, B.; Flint, D. J.; Plumb, J. A.; Graham, D.; Wheate, N. J. *J. Am. Chem. Soc.* **2010**, *132*, 4678.
- (17) Dhar, S.; Daniel, W.; Gijohann, D. A.; Mirkin, C. A.; Lippard, S. J. *J. Am. Chem. Soc.* **2009**, *131*, 14652.
- (18) Min, Y.; Mao, C.; Xu, D.; Wang, J.; Liu, Y. *Chem. Commun.* **2010**, *46*, 8424.
- (19) Ren, L.; Huang, X.-L.; Zhang, B.; Sun, L.-P.; Zhang, Q.-Q.; Tan, M.-C.; Chow, G.-M. *J. Mater. Biomed. Res. A* **2008**, *85*, 787.
- (20) Xu, C.; Wang, B.; Sun, S. *J. Am. Chem. Soc.* **2009**, *131*, 4216.
- (21) Brust, M.; Walker, M.; Bethell, D.; Schiffrin, D. J.; Whyman, R. *J. Chem. Soc., Chem. Commun.* **1994**, 801.
- (22) Kimling, J.; Maier, M.; Okenve, B.; Kotaidis, V.; Ballot, H.; Plech, A. *J. Phys. Chem. B* **2006**, *110*, 15700.
- (23) Perrault, S. D.; Chan, W. C. W. *J. Am. Chem. Soc.* **2009**, *131*, 17042.
- (24) Ji, X.; Song, X.; Li, J.; Bai, Y.; Yang, W.; Peng, X. *J. Am. Chem. Soc.* **2007**, *129*, 13939.
- (25) Brown, K. R.; Daniel, G. W.; Natan, M. J. *Chem. Mater.* **2000**, *12*, 306.
- (26) Frens, G. *Nat. Phys. Sci.* **1973**, *241*, 20.
- (27) Ji, X.; Song, X.; Li, J.; Bai, Y.; Yang, W.; Peng, X. *J. Am. Chem. Soc.* **2007**, *129*, 13939.
- (28) Sutton, D.; Nasongkla, N.; Blanco, E.; Gao, J. *Pharm. Res.* **2007**, *24*, 1029.
- (29) Kim, C.-K.; Ghosh, P.; Rotello, V. M. *Nanoscale* **2009**, *1*, 61.
- (30) Reiter, W. J.; Pott, K. M.; Taylor, K. M. L.; Lin, W. *J. Am. Chem. Soc.* **2008**, *130*, 11584.
- (31) Dougan, J. A.; Karlsson, C.; Smith, W. E.; Graham, D. *Nucleic Acids Res.* **2007**, *35*, 3668.
- (32) BBInternational. Gold nanoparticle extinction coefficients. Personal communication, 2010.
- (33) Famulok, M.; Mayer, G. *Nature* **2006**, *439*, 666.
- (34) Chandran, P. R.; Naseer, M.; Udupa, N.; Sandhyarani, N. *Nanotechnology* **2012**, *23*, 015602.
- (35) Ivanov, M. R.; Bednar, H. R.; Haes, A. J. *ACS Nano* **2009**, *3*, 386.
- (36) Link, S.; El-Sayed, M. A. *J. Phys. Chem. B* **1999**, *103*, 4212.
- (37) Xie, J.; Xu, C.; Kohler, N.; Hou, Y.; Sun, S. *Adv. Mater.* **2007**, *19*, 3163.
- (38) Budijono, S. J.; Russ, B.; Saad, W.; Adamson, D. H.; Prud'homme, R. K. *Colloids Surf., A* **2010**, *360*, 105.
- (39) Cho, W.-S.; Cho, M.; Jeong, J.; Choi, M.; Cho, H.-Y.; Han, B. S.; Kim, S. H.; Kim, H. O.; Lim, Y. T.; Chung, B. H.; Jeong, J. *Toxicol. Appl. Pharmacol.* **2009**, *236*, 16.
- (40) Mei, B. C.; Oh, E.; Susumu, K.; Farrell, D.; Mountziaris, T. J.; Mattoussi, H. *Langmuir* **2009**, *25*, 10604.
- (41) Liu, Y.; Shipton, M. K.; Ryan, J.; Kaufman, E. D.; Franzen, S.; Feldheim, D. L. *Anal. Chem.* **2007**, *79*, 2221.
- (42) Pons, T.; Uyeda, H. T.; Medintz, I. L.; Mattoussi, H. *J. Phys. Chem. B* **2006**, *110*, 20308.
- (43) Lu, Q. B.; Kalantari, S.; Wang, C. R. *Mol. Pharm.* **2007**, *4*, 624.
- (44) Gittins, D. I.; Caruso, F. *Adv. Mater.* **2000**, *12*, 1947.
- (45) Wu, L.; Zhang, J.; Watanabe, W. *Adv. Drug Delivery Rev.* **2011**, *63*, 456.
- (46) Balasubramanian, S. K.; Yang, L.; Yung, L.-Y. L.; Ong, C.-N.; Ong, W.-Y.; Yu, L. E. *Biomaterials* **2010**, *31*, 9023.
- (47) Lippert, B. *Platinum Nucleobase Chemistry. Progress in Inorganic Chemistry*; John Wiley & Sons, Inc.: New York, 2007.